Volume 139 | Number 11 | 7 June 2014 | Pages 2603–2920

Analyst

www.rsc.org/analyst

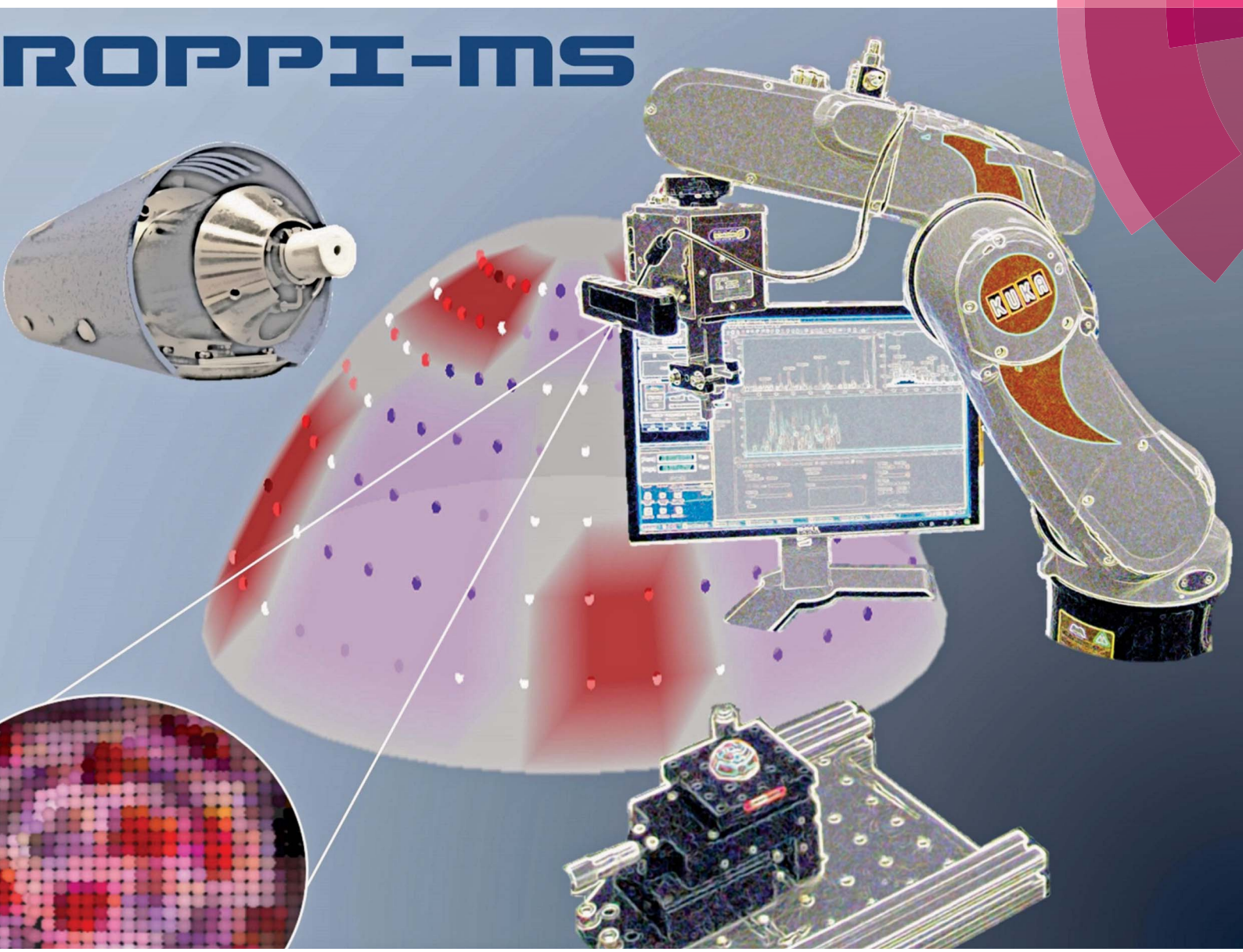

ISSN 0003-2654

ROYAL SOCIETY OF CHEMISTRY

COMMUNICATION
Facundo M. Fernández *et al.*
Robotic plasma probe ionization
mass spectrometry (RoPPI-MS) of non-planar surfaces

Analyst

COMMUNICATION

View Article Online
View Journal | View Issue

Robotic plasma probe ionization mass spectrometry (RoPPI-MS) of non-planar surfaces†

Cite this: *Analyst*, 2014, **139**, 2658

Received 7th February 2014
Accepted 27th February 2014

DOI: 10.1039/c4an00277f

www.rsc.org/analyst

Rachel V. Bennett,‡[a] Ezequiel M. Morzan,§‡[a] Jacob O. Huckaby,[b] María Eugenia Monge,¶[a] Henrick I. Christensen[b] and Facundo M. Fernández*[a]

In this report, we present a robotic sample introduction/ionization system for mass spectrometry (MS) for spot analysis and imaging of non-planar surfaces. The system operates by probing the sample surface with an acupuncture needle, followed by direct plasma chemical ionization time-of-flight MS.

With the development of ambient ionization techniques,[1] mass spectrometry imaging (MSI) has evolved into a powerful surface analysis tool.[2] During a microprobe ambient MSI experiment, mass spectral data is acquired as a function of time while the spatial information is also recorded. Then, through the time domain, the MS data is correlated with spatial position to create a chemical image. Image resolution for MSI data is generally determined by the beam size impacting the surface (*e.g.* laser spot, spray plume, ion beam, *etc.*). More specific spatial information is obtained with higher spatial resolution but at the cost of sensitivity; *i.e.*, a smaller sampled area allows less material to be desorbed/ablated and detected.

Vacuum-based ionization techniques such as matrix-assisted laser desorption/ionization (MALDI)[3] or secondary ion mass spectrometry (SIMS)[4] provide high spatial resolution images (~10 μm or 100 nm, respectively), but require thin planar samples. Ambient MSI methods are less restricted by sample size and shape, offering convenience through reduced sample preparation. These include spray-based techniques that comprise a solid–liquid extraction followed by electrospray ionization as in the case of desorption electrospray ionization (DESI)[5,6] and the liquid microjunction surface sampling probe (LMJ-SSP).[7] Laser ablation can be coupled to various ionization sources for imaging, as in laser ablation-electrospray ionization (LAESI)[8] or infrared laser ablation-metastable-induced chemical ionization (IR-LAMICI),[9] among others.[2] Alternatively, sampling of a surface decoupled from the ionization event can be achieved using a small probe, such as the solid needle used in probe electrospray ionization (PESI)[10,11] which laid the foundation for our work.

MSI data is typically acquired for 2-dimensional planar samples, given the need for consistent probe-surface-inlet geometry. MSI analysis of more complex objects can be performed in one of the following ways: (1) 2D imaging of serial sample sections followed by computer rendering into a 3D image or (2) serial imaging of surface layers by sequential depth profiling or sputtering across an area.[12] The first method is commonly used in the 3D imaging of biological tissues and is amenable to all imaging methods.[13] The second is typically performed with a more ablative method, such as LAESI or SIMS, on thicker samples.[14,15] Both approaches ultimately produce a full 3D volumetric image with information about the sample interior, but require long (≥40 hours) analysis times, and several sample preparation steps.[16]

In this work, we present a method for the systematic 3D surface analysis of native, irregularly-shaped or curved samples by coupling robotic probe surface sampling with direct analysis in real time (DART).[17] DART was selected as a plasma-based ionization source for its ability to ionize both polar and non-polar analytes[18] and its relatively large ionization region.[19] The large range of ionizable analytes and the implementation of a robotic probe broaden the possible applications of this new surface analysis technique, and allow for remote sampling. For example, this system would be conducive to the real-time analysis of metabolites in biological samples, as in the case of tissue screening during

[a]*School of Chemistry and Biochemistry, Georgia Institute of Technology, 901 Atlantic Dr. NW, Atlanta, GA, USA. E-mail: facundo.fernandez@chemistry.gatech.edu; Fax: +1 (404)894-7452; Tel: +1 (404)385-4432*

[b]*Institute for Robotics and Intelligent Machines, Georgia Institute of Technology, Atlanta, GA, USA*

† Electronic supplementary information (ESI) available: Video of RoPPI-MS analysis sequence. See DOI: 10.1039/c4an00277f

‡ These authors contributed equally to this body of work.

§ Current address: Laboratorio de Análisis de Trazas, INQUIMAE, Facultad de Ciencias Exactas y Naturales, Universidad de Buenos Aires, Buenos Aires, Argentina.

¶ Current address: Centro de Investigaciones en Bionanociencias (CIBION), Consejo Nacional de Investigaciones Científicas y Técnicas (CONICET), Godoy Cruz 2390, C1425FQD, Ciudad de Buenos Aires, Argentina.

surgery to differentiate between healthy and tumour regions for biopsy, given the rather non-invasive nature of the acupuncture needle. The larger ionization region accommodates minor precision errors in the robotic placement of the sample probe while still allowing for efficient ionization. Another advantage of coupling the robotic probe with DART is that the sample does not need to contain a certain amount of water or other fluids for effective ionization as in the case of PESI[10] due to the inherent ionization mechanisms of plasma-based sources.[1,17]

Two different robotic arms were utilized for proof-of-principles experiments: a do-it-yourself Lynxmotion AL5A-5 and a Kuka KR5 sixx R650 robot. Fig. 1 schematically illustrates the analysis process of this method with the Kuka robot when sampling dye-coloured spots on a hand-painted polystyrene hemisphere as a test sample. Starting at a "home position" (Fig. 1a), a robotic arm manoeuvres an acupuncture needle to stab the surface of the sample, which is mounted remotely outside the ionization region, thus collecting a small amount of analyte (Fig. 1b). This is similar to the initial step in the PESI[10] process, but robot-assisted. The needle is then reproducibly inserted into the ionizing gas stream of the DART ion source (Fig. 1c). The position sampled by the robotic probe may be selected by means of a joystick control, or by using a 3D camera (Fig. 1f) that creates an (x, y, z) point cloud (Fig. 1g) for accurate sample coordinate determination. A selected ion chronogram observed for each of the analysis steps described, and the subsequent mass spectrum are shown in Fig. 1d and e. By probing multiple points across the sample surface, the acquired mass spectra (and corresponding peak areas from extracted ion chronograms) are correlated with the known x, y, and z position. We have named this approach robotic plasma probe ionization-mass spectrometry (RoPPI-MS).

The total analysis time in RoPPI-MS is dependent upon three factors: robot speed, number of surface points, and desorption/ionization time of the analytes from the needle. In the current configuration, the latter of these is the slowest step (on the order of minutes), and thus the speed-limiting variable as it depends on the time for the signal to return to the baseline ensuring no carryover between samples. The duration of this step can be optimized by changing the temperature of the DART gas stream to induce faster exhaustive sample consumption. In order to optimize the DART temperature for ideal operation, a planar polystyrene surface was coloured with black Sharpie. The surface was robotically probed and the base peak signal (m/z 303.4819) was recorded for different positions in the ionization region, and various DART temperatures between 200 and 400 °C. Maximum sensitivity was observed when the acupuncture needle tip was placed within 1 mm of the DART nozzle, the hottest region of the gas stream.[19] As expected, at higher temperatures a faster analyte desorption was achieved, resulting in sharper signals. Indeed, the highest signal intensity was observed at 400 °C with negligible thermally-induced analyte fragmentation. Therefore, 400 °C was chosen as the DART operating temperature for further experiments, enabling higher throughput analysis.

The need for higher desorption temperatures than those typically utilized in DART-MS with glass sampling probes, is attributed to the thermal conductivity of stainless steel, which is 15× higher than glass.[20] Glass melting point capillaries are common sampling tools for DART because they efficiently maintain heat at the tip of the capillary where the sample is

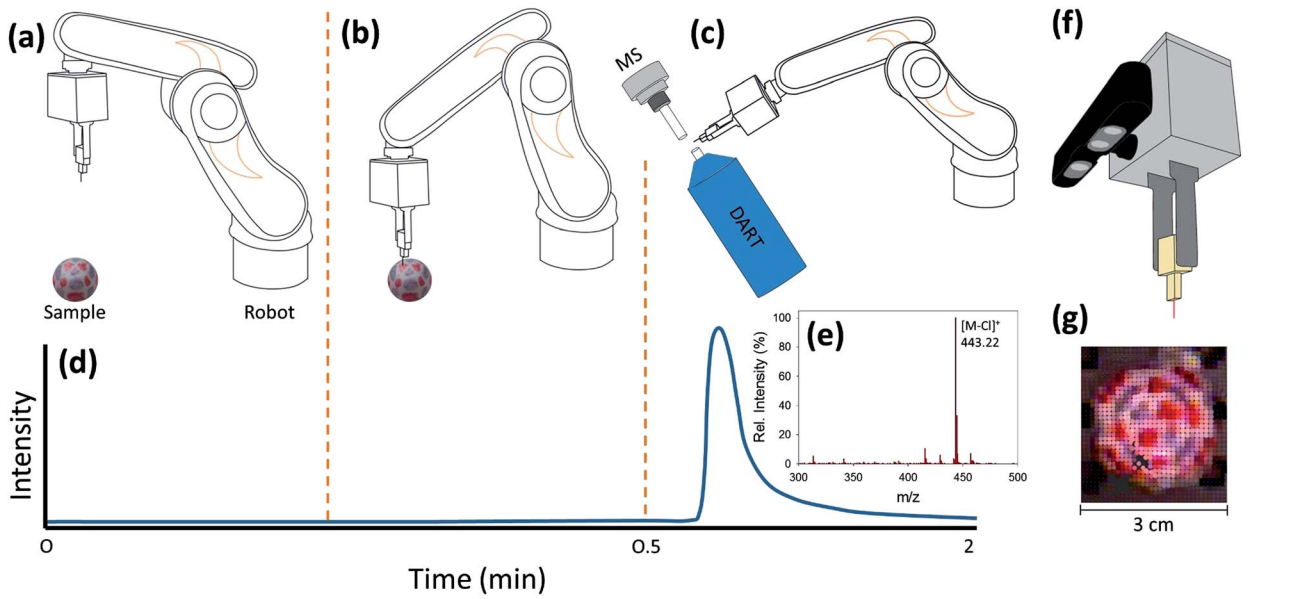

Fig. 1 Robot in the home position (a), sampling position (b), and analysis position in which the needle is placed between the DART ion source and MS gas-ion-separator (GIST) interface (c). Selected ion intensity chronogram at m/z 443 ($[M - Cl]^+$ for rhodamine 6G) observed during the analysis sequence corresponding to the robot positions described directly above (d). Sample mass spectrum observed during analysis of rhodamine 6G coloured spots (e). End effector (grey), PEEK needle mount (tan), acupuncture needle (red) and 3D visualization camera (black) (f) for point cloud generation (g).

localized for desorption. In contrast, the higher thermal conductivity of the stainless steel results in faster heat dissipation across the needle and thus less effective vaporization of the analytes on the tip. The small mass of an acupuncture needle further favours heat dissipation in comparison to the larger glass capillary. The higher DART analysis temperature is not only necessary for faster analysis times, but also beneficial to prevent carryover between sampling points. In the current system configuration, the motion sequence is manually initiated for each sampled point when the total ion trace returns to baseline intensity, indicating all analyte has been desorbed and no sample is being carried over to subsequent analyses.

The do-it-yourself Lynxmotion AL5A-5 robotic arm was used in the first set of experiments, and comprised 5 degrees of freedom and motion precision of ~5 mm. To enhance accurate surface analysis, only two arm degrees of freedom were used, which improved precision to 3 mm. With this system, the sample was mounted on a 3-axis RollerBlock with micrometre drives with 0.01 mm precision to control sampling position. The robot was programmed to sample one specific x, y, z coordinate orthogonal to the sample stage, and the RollerBlock moved the sample so that new regions of the sample surface were probed. Manual control of the sample stage allowed for simplified robot programming by repeating one motion sequence. For this set of experiments, the polystyrene hemisphere (13 mm diameter, shown in Fig. 2a) used as test sample was painted with rhodamine 6G (m/z 443.2335) and Nile Blue Chloride (m/z 318.3645) in three rows of eight equally-spaced spots.

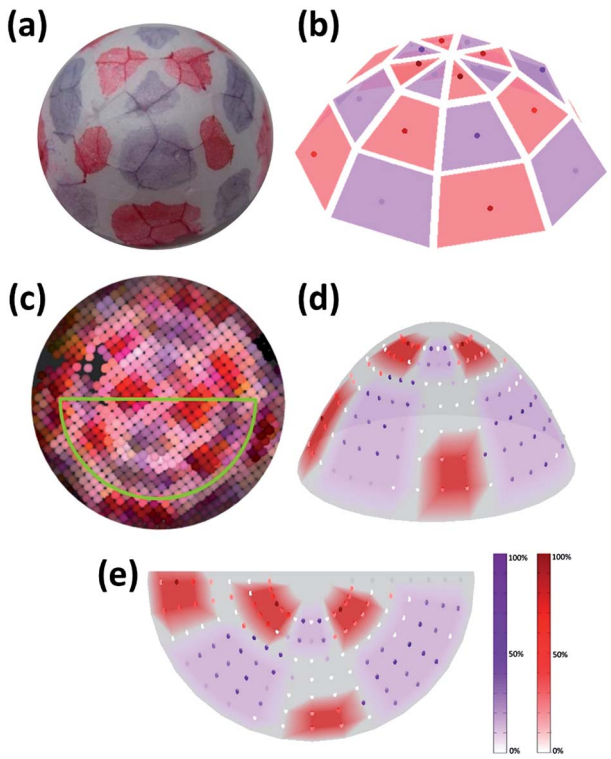

Fig. 2 (a) Optical image of small polystyrene hemisphere imaged by sampling one point per dye spot and (b) corresponding RoPPI-MS image. (c) 3D point cloud top-view of large polystyrene hemisphere with area sampled outlined in green, (d) top-view of RoPPI-MS image, and (e) side-view of RoPPI-MS image acquired; grey areas in (d) and (e) were not sampled. Data for (b) was acquired with the Lynxmotion robot whereas data for (d) and (e) was acquired with the Kuka robot.

The theoretical limit of the spatial resolution of this technique is determined by the diameter of the sampling probe, which in this case is an acupuncture needle of 180 μm. However, the Lynxmotion robotic arm limits the spatial resolution to ~3 mm. For this reason, preliminary experiments were carried out by sampling only one point for each colour painted block on the polystyrene hemisphere (Fig. 2a). By puncturing the surface to a depth of ~2 mm, this simple proof-of-principle setup afforded sufficient sensitivity, but with significant resolution limitations.

Mass spectral data is converted into a 3D chemical information mesh by integrating the extracted peak area from each sampled point and pairing that with the x, y, z coordinates. This information is plotted using the *scatter3* function in Matlab® and translating sampling coordinates to points on the mesh of the hemisphere created (Fig. 2b–e). As the area sampled by the acupuncture needle is smaller than the sample spacing (1 mm), the signal observed was plotted as circles whose diameter reflect the precision of the measurement. These points are overlaid on a hemisphere showing the theoretical distribution of the dye painted on the surface. Peak area was converted into a pseudocolour intensity map used in the fill of each data spot. For ease of visualization of the dye data, two separate scale bars were set within the primary colourmap for each colour component painted on the surface. For all data shown here, the purple scale denotes the ion intensity for Nile Blue Chloride and the red scale corresponds to rhodamine 6G.

Following these early experiments, the Kuka KR5 sixx R650 robot (Fig. 1a) was implemented. This higher-precision robot comprised 6 degrees of freedom, a greater range of motion (650 mm) to accommodate larger samples, and motion precision of 0.02 mm. This robotic system was paired with a 3D point cloud visualization system mounted on the robot arm (Fig. 1f) to allow for user-selectable sampling position (Fig. 1b). In between each point of analysis, the robot returns to the home position hovering above the sample (Fig. 1a) to allow the user to select a new point in the 3D point cloud image. Given a constant home position, the point cloud generated is the same for each analysis sequence, which facilitates full surface coverage. Although the robotic arm has a precision of 0.02 mm, which defines the maximum resolution of the technique, the resolution of the current 3D point cloud limits sampling to points with 1 mm spacing. The sampling and analysis process of this new system may be viewed as a video included in the ESI.†

Using the 3D vision system input, the new x, y, z coordinate is specified for each analysis sequence so that the robot automatically probes the new position. This eliminates the need for manual adjustment of the sample position as in the early experiments because the robot is now easily capable of precise motion across the entire surface through more advanced programming. Given the defined home position, the robot still probes the sample surface orthogonal to the sample stage resulting in various approach angles, but the accuracy of the robot motion is sufficient to ensure reproducible sampling.

Despite these improvements in the sophistication of the method, the 3D sensor is limited in the *z* dimension resolution (0.10 cm at optimal configuration), which often results in a noisy point cloud generation, particularly at surface boundaries. Even so, the depth to which the acupuncture needle punctures the surface is still more precise with this combination of vision system and robot than manual adjustment of the sample (puncture depths ranging from 1–5 mm).

This second set of 3D surface sampling experiments was conducted on a larger polystyrene hemisphere (30 mm diameter) that was also hand-painted with the same dyes. The top-down view seen through the 3D vision system and the sampled area are illustrated in Fig. 1g and 2c, respectively. This sampled area resulted in 128 evenly-distributed data points that were also plotted using Matlab® following the same procedure described above (Fig. 2d and e). The variable intensity detected within each painted region and the irregularly-shaped boundaries are mainly attributed to the hand painting of the sample. The detection of dye ions outside the intentionally painted areas of the surface is attributed to the bleeding of the dye solution along crevices in the polystyrene. These studies indicate the second robotic system provides the most accurate 3D chemical images of curved surfaces.

Materials and methods

A DART source (Ion Sense, model SVP100) coupled to a Q-TOF mass spectrometer (Bruker micrOTOF-QII) was used for all the measurements in positive ion mode using He as the discharge supporting gas (1 L min^{-1}). The set DART gas temperature was varied between 200 and 400 °C to determine the effects of the temperature on the shape of the ion trace. The glow discharge needle voltage of the DART source was set to −3500 V. Millenia stainless steel acupuncture needles (0.18 mm × 13 mm) were used for surface sampling by mounting them on a custom-made PEEK block which was tightly held by the robot gripper.

The first robotic arm used in the set-up was a Lynxmotion AL5A (Swanton, VT, USA) with 5 degrees of freedom. The median reach of the arm was 14.60 cm with a 113.40 g lift capacity. Only the wrist and the base actuators were used in order to maximize precision. The robot was manually moved to define home, sampling and analysis positions which were then saved into a motion path program (Lynxmotion RIOS SSC-32 V1.06). This sequence was repeated for each sampling position on the hemisphere with constant home, sampling and analysis positions, and the sample was manually moved using the 3-axis RollerBlock (ThorLabs, Newton NJ).

The second manipulator used was a KUKA KR5 sixx R650 robot (Shelby Township, MI, USA), a platform targeted toward light manufacturing and industrial tasks. It has 6 degrees of freedom with a maximum reach of 650 mm, a payload of 5 kg, and a maximum speed of 7.6 m s^{-1}. Motion control of the robot was programmed using a custom Robot Operating System (ROS) interface to the KUKA controller. Robot perception was performed using a PrimeSense (San Jose, CA, USA) Carmine 1.09 short range 3D sensor mounted to the end effector of the robot, just above the sampling rig, calibrated to the reference frame of the robot, and the Point Cloud Library (PCL) software package. Using techniques from computer vision, the library takes data from the sensor and creates a 3D point cloud of the environment. The RViz visualization software (also available from ROS) was utilized to visualize that point cloud of the scene, and provide an interface for the human operator to specify a location on the surface for the robot to sample. After peak area was extracted from extracted ion chronograms, all images were rendered in Matlab® (Mathworks, Natick, MA, USA).

Conclusions

A new mass spectrometry surface analysis technique, RoPPI-MS, is first described for the investigation of non-planar samples. The use of an ionization technique without enclosures such as DART enables easy and repeatable injections of the probed material into the plasma region. RoPPI-MS opens new avenues for examining *in vivo* tissues, organisms as they grow, classifying human skin lesions, probing 3D cell cultures, high-throughput baggage screening, monitoring produce safety, *etc.* We recognize that the resolution in the current system can still be improved, mainly arising from limitations of the robotic arms utilized. This is not a drawback of the concept *per se*, but of the specific implementation used in these proof-of-principle experiments. We are currently implementing a new RoPPI-MS system with a robotic arm with 0.1 mm positioning repeatability, and a tangent-to-surface probe stabbing approach to further improve surface sampling. Extensive characterization of the analytical figures of merit of this system will be reported in the future.

Acknowledgements

This work was supported by ARRA NSF MRI Instrument Development grant #0923179 to FMF and the NSF and NASA Astrobiology Program under the NSF Center for Chemical Evolution CHE-1004570.

References

1 M. E. Monge, G. A. Harris, P. Dwivedi and F. M. Fernández, *Chem. Rev.*, 2013, **113**, 2269–2308.
2 C. Wu, A. L. Dill, L. S. Eberlin, R. G. Cooks and D. R. Ifa, *Mass Spectrom. Rev.*, 2013, **32**, 218–243.
3 R. M. Caprioli, T. B. Farmer and J. Gile, *Anal. Chem.*, 1997, **69**, 4751–4760.
4 M. L. Pacholski and N. Winograd, *Chem. Rev.*, 1999, **99**, 2977–3006.
5 G. J. Van Berkel and V. Kertesz, *Anal. Chem.*, 2006, **78**, 4938–4944.
6 J. M. Wiseman, D. R. Ifa, Q. Song and R. G. Cooks, *Angew. Chem., Int. Ed.*, 2006, **45**, 7188–7192.
7 G. J. Van Berkel, V. Kertesz, K. A. Koeplinger, M. Vavrek and A.-N. T. Kong, *J. Mass Spectrom.*, 2008, **43**, 500–508.
8 P. Nemes, A. A. Barton, Y. Li and A. Vertes, *Anal. Chem.*, 2008, **80**, 4575–4582.

9 A. S. Galhena, G. A. Harris, L. Nyadong, K. K. Murray and F. M. Fernández, *Anal. Chem.*, 2010, **82**, 2178–2181.
10 K. Hiraoka, K. Nishidate, K. Mori, D. Asakawa and S. Suzuki, *Rapid Commun. Mass Spectrom.*, 2007, **21**, 3139–3144.
11 L. C. Chen, K. Yoshimura, Z. Yu, R. Iwata, H. Ito, H. Suzuki, K. Mori, O. Ariyada, S. Takeda, T. Kubota and K. Hiraoka, *J. Mass Spectrom.*, 2009, **44**, 1469–1477.
12 E. H. Seeley and R. M. Caprioli, *Anal. Chem.*, 2012, **84**, 2105–2110.
13 A. C. Crecelius, D. S. Cornett, R. M. Caprioli, B. Williams, B. M. Dawant and B. Bodenheimer, *J. Am. Soc. Mass Spectrom.*, 2005, **16**, 1093–1099.
14 J. S. Fletcher, N. P. Lockyer, S. Vaidyanathan and J. C. Vickerman, *Anal. Chem.*, 2007, **79**, 2199–2206.
15 P. Nemes, A. A. Barton and A. Vertes, *Anal. Chem.*, 2009, **81**, 6668–6675.
16 L. S. Eberlin, D. R. Ifa, C. Wu and R. G. Cooks, *Angew. Chem., Int. Ed.*, 2010, **49**, 873–876.
17 R. B. Cody, J. A. Laramée and H. D. Durst, *Anal. Chem.*, 2005, **77**, 2297–2302.
18 R. B. Cody, *Anal. Chem.*, 2009, **81**, 1101–1107.
19 G. A. Harris and F. M. Fernández, *Anal. Chem.*, 2009, **81**, 322–329.
20 *CRC Handbook of Chemistry and Physics*, CRC Press, Inc., Boca Raton, FL, 62nd edn, 1981.